Applied Thermal Engineering 126 (2017) 315–321

Contents lists available at ScienceDirect

Applied Thermal Engineering

journal homepage: www.elsevier.com/locate/apthermeng

Research Paper

Numerical study of the influence of tube arrangement on the flow distribution in the header of shell and tube heat exchangers

O. Labbadlia [a,*], B. Laribi [a], B. Chetti [a], P. Hendrick [b]

[a] Faculty of Science and Technology, University of Djilali Bounaama Khemis Miliana, Khemis Miliana 44225, Algeria
[b] Service Aéro-Thermo-Mécanique, Université Libre de Bruxelles (ULB), Brussels 1050, Belgium

HIGHLIGHTS

- The influence of tubes arrangement on the flow distribution has been investigated.
- Four arrangements types, in a shell and tube heat exchanger, have been studied.
- Tubes arrangement type directly affect the flow distribution.
- The 45° arrangement ensures a high velocity at maximum number of tubes.
- The 60° arrangement provides the best flow distribution uniformity.

ARTICLE INFO

Article history:
Received 28 February 2017
Revised 13 July 2017
Accepted 25 July 2017
Available online 27 July 2017

Keywords:
Shell and tube heat exchanger
Flow maldistribution
CFD

ABSTRACT

The behavior of the fluid inside the internal circulation system of a shell and tube heat exchanger is complex due to the influence of many factors. The flow distribution has a significant influence on the performance of fluidic apparatus such as shell and tube heat exchangers. The non-uniformity of the flow distribution reduces the efficiency of the process. The influence of tubes arrangements on the flow distribution is presented using CFD simulations. In this study, four arrangement types are considered. The present results are in good agreement with those of the literature. The obtained results show that the arrangement of the tubes has a significant influence on the flow distribution. It was concluded that the flow distribution of 60° arrangement exhibits better uniformity compared to the conventional arrangement (90°) by 21%. The 45° arrangement gives good uniformity of pressure distribution compared to the other arrangements.

1. Introduction

Heat exchangers are devices that allow the transfer of thermal energy between two fluids, a rather critical operation in many processes. They are widely used within the chemical, pharmaceutical and petro-chemical industries, in power stations and in many other applications [1,2]. Several types of heat exchangers exist and choosing the appropriate type for a given process is not a trivial procedure [3]. In fact, it is commonly known that selecting the wrong type for a given plant can lead to sub-optimal performance, operability issues and equipment failure [4]. One frequently used type is the tubular heat exchanger, which has the advantage of offering a large heat transfer surface and a compact design. The key design aspect of this type of exchangers is to make the distribution of the flow as uniform as possible [4,5]. The non-uniformity is one of the main causes that are known to significantly degrade the performance of the heat exchangers.

Limited works have been achieved in the field of flow distribution within a dividing inlet manifold of a tubular heat exchanger. Acrivos et al. [6] predicted that the downstream conditions have no influence in the determination of the lateral flow in the upstream tubes. They have also indicated that a wider cross-sectional area at the collectors, will further improve the flow distribution. Kubo and Ueda [7] found that the flow distribution quality is independent of the Reynolds number range between 30,000 and 100,000, and that the flow distribution will be improved if the resistance of branch tubes are increased. Furthermore they have reported that better flow distribution will be obtained if a larger cross sectional area is to be used. Rohsenow and Putnam [8] found that the maldistribution and unstable flows are more likely to occur in laminar flows than in turbulent flows. Kuppan [9] reported that the use of a small pitch would give a greater heat transfer in

* Corresponding author at: 52 Cadat, Khemis Miliana 44225, Algeria.
E-mail address: o.labbadlia@univ-dbkm.dz (O. Labbadlia).

http://dx.doi.org/10.1016/j.applthermaleng.2017.07.184
1359-4311/

Nomenclature

a_1	*SST* turbulence model constant
d	the distance from the field point to the nearest wall, m
D	manifold diameter, m
D_n	nominal diameter, m
g	gravitational body force, $m^3/kg\ s^2$
k	turbulence kinetic energy, m^2/s^2
L	head length, m
M	the ratio of the sum of all port areas to header area
N	the maximum number of tubes with a certain velocity deviation interval of $\pm\bar{\varepsilon}$
n	total number of tubes
P	manifold pressure, Pa
ΔP_c	pressure differential for the cold fluid, Pa
ΔP_h	pressure differential for the hot fluid, Pa
ΔP_t	pressure difference, Pa
Re	Reynolds number
U	velocity, m/s
U_i	velocity at the tube i, m/s
U_m	mean velocity, m/s
υ_T	turbulent viscosity, Pa s
W_{ij}	the vorticity tensor
x, y	spatial coordinates, m

Greek Symbols

β_1	k- ω turbulence model constant
β_2	k-ε turbulence model constant
β^*	*SST* turbulence model constant
δ	identity matrix or Kronecker Delta function
ε_i	velocity deviation
υ	kinematic viscosity, m^2/s
ρ	density, kg/m^3
σ_{k1}	k- ω turbulence model constant
σ_{k2}	k-ε turbulence model constant
$\sigma_{\omega1}$	k- ω turbulence model constant
$\sigma_{\omega2}$	k-ε turbulence model constant
τ	shear stress, N/m^2
ω	specific dissipation rate, $1/s$
Ω	the vorticity magnitude, $1/s$

Subscripts

c	cold fluid
h	hot Fluid
i	tube number
n	nominal
m	mean
t	total
T	turbulent

the shell side and results in more surface compactness. However, the use of a large pitch will provide greater reduction in the pressure drop and in the fouling at the shell. Mohan et al. [10] found that the flow maldistribution is a function of the number of tubes, the flow rate and the tube size. Hewitt and Barbosa [11] mentioned that, to some extent, it is possible to quantify the maldistribution of gross flows in a turbulent flow by relating it to both the total pressure drop through the tubes bank and to the dynamic energy of the fluid at the inlet of the head. Lu et al. [12] developed a discrete model for calculating the flow distribution in the collectors. Saber et al. [13] indicated that the increase in the total pressure loss is due to the increase in kinetic energy of the fluid. Li-Zhi Zhang investigated the flow maldistribution and thermal performance deterioration in cross-flow air to air heat exchangers [14] and in a parallel plates membrane core case [15], he found that as long as the pitch is smaller the flow distribution is quite homogenous and the thermal deterioration due to flow maldistribution can be neglected. The flux in the dividing collectors was formulated by a standard equation by the works of Wang [16,17]. Rebrov et al. [18] demonstrated that the 3D digital model will correctly predict the flow distribution. Venkatesan [19] indicated that the uniformity of the flow distribution is inversely proportional to the length of the head. In fact, a lengthier head, will result in a more non-uniform flow distribution. The static pressure will be almost equal for all pipes in the case of a conical head. Bhutta et al. [20] focused on the applications of computational fluid dynamics (CFD) in the field of heat exchangers. They have found that the CFD was used in different fields of study like the maldistribution of fluid flows. These simulations have generated largely accurate solutions, showing that the CFD is a very effective tool to predict the behavior and performance of a wide variety of heat exchangers. Gandhi et al. [21] showed that the uniformity of the distribution is a function of both the geometry of the manifold, and the kinetic energy input. They also indicated that the uniformity of flow distribution was obtained by reducing the tube diameter, and that at a constant value of the Reynolds number, all the working fluids (air/water) have the same effect on the extent of the non-uniformity for the configurations considered in this work. Li-Zhi Zhang et al. [22], Zhen-Xing Li and Li-Zhi Zhang [23] investigated the flow maldistribution and the consequent performance deteriorations in a cross flow and in a counter flow hollow fiber membrane module, they found that the packing fraction affects the flow maldistribution substantially. Mohammadi and Malayeri [24] proved that the maldistribution in the turbulent regime is not a function of Reynolds number, but it depends considerably on the geometrical characteristics of the heat exchanger regardless of the exchanger type. They reported that the flow maldistribution is a function of the number of tubes, i.e., until the number of tubes increases, the uniform distribution or the maximum number of tube with a velocity deviation less than |5%| also increases.

It can be seen from the previous researches that the geometrical parameters affect the flow distribution in the shell and tube heat exchangers. The novelty of this work is to investigate the effect of the tubes arrangements on the flow distribution using CFD tools.

2. Modeling and simulation

In this study, CFD tools are used to simulate the flow at the head of a tubular heat exchanger in order to investigate the influence of the tube arrangement on the distribution of the fluid (Fig. 1a and b).

2.1. Physical model

The selected exchanger is an industrial medium type (Fig. 1), it contains a single pass with 464 and 461 tubes for the two cases of 90° and 45° arrangements respectively. For the 30° and 60° arrangements, the heat exchanger has a single pass with 517 and 465 tubes respectively (Fig. 2). The geometric characteristics values of the heat exchanger are shown in Table 1.

2.2. Governing equations

For the case of a steady flow, the continuity and the momentum equations are expressed as follows:

$$\nabla.(\rho\vec{v}) = 0 \tag{1}$$

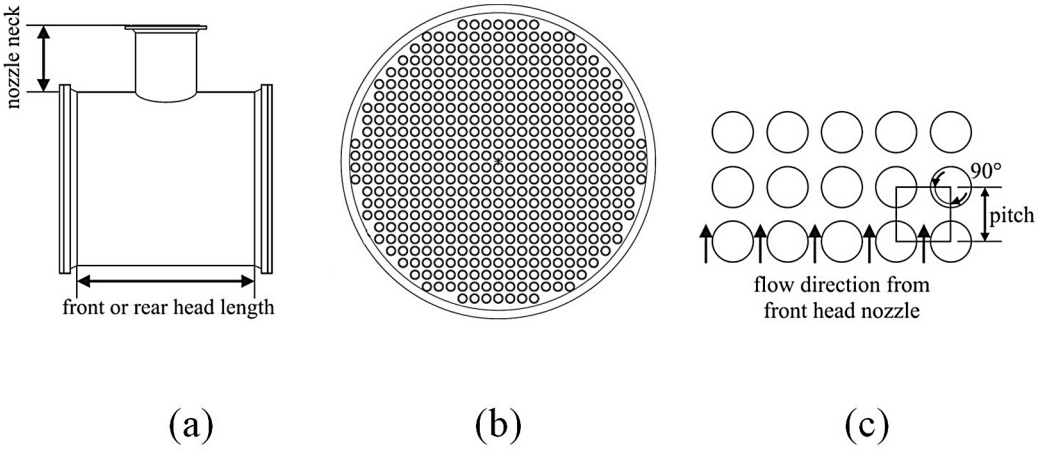

Fig. 1. Typical geometric configuration of a medium industrial tubular heat exchanger [24].

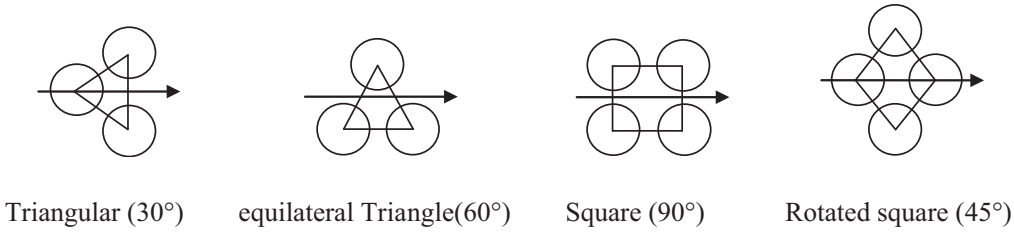

Fig. 2. Different tubes arrangements.

Table 1
Geometric characteristics of the exchanger.

Designation	Value
Diameter of the head (mm)	838.20
Length of the head (mm)	628.65
Neck Length (mm)	377
Diameter of the neck (mm)	387
Tube Diameter (mm)	25.40
Pitch (mm)	31.75
Number of tube for 90°/60°/45°/30°	464/465/461/517

where υ is the dynamic viscosity

$$\nabla.(\rho\vec{v}\vec{v}) = -\nabla P + \nabla.(\bar{\bar{\tau}}) + \rho\vec{g} \quad (2)$$

where τ is the shear stress, g is the gravitational body force

2.3. Mesh generation

The computational domain is meshed with an unstructured mesh Tet/hybrid, which is generated with the Gambit commercial code. A mesh independence test is carried out with different numbers of nodes with a special focus on the tube inlet. The independence is obtained with more than 8 million cells (Fig. 3). The number of nodes is increased for each tube inlet until it reached 85 nodes. The number of cells obtained after a good refining mesh is given in Table 2 for each type of arrangement. The mesh quality of a complete domain is very good since up to 90% of all cells have a skew value equal to 0.45 and they are not higher than 0.7.

where $\boldsymbol{N}/\boldsymbol{n}$ is the ratio of the number of tubes at known velocity deviation to the total number of tubes.

2.4. Turbulence model

The shear-stress transport k-ω SST model is selected as turbulence model since this model significantly improves the accuracy

Table 2
Size of the mesh.

Type	Grid size
90°	8 887 743
60°	8 852 851
45°	8 846 324
30°	8 932 483

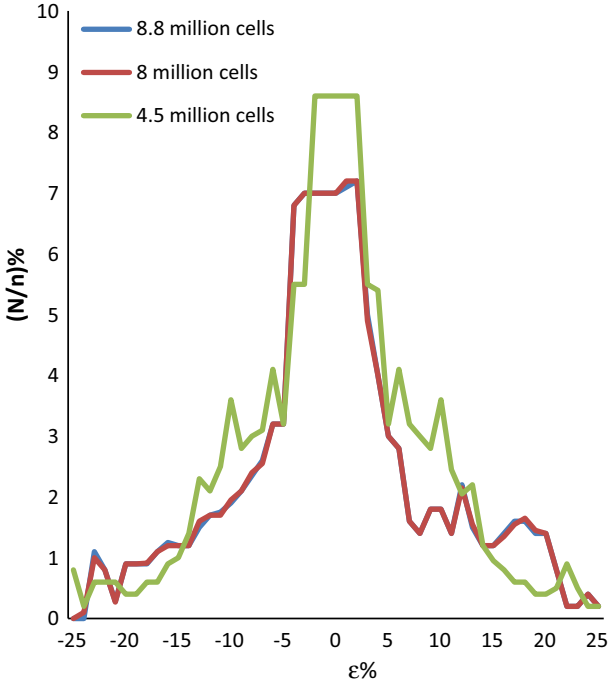

Fig. 3. Study of the mesh independence.

for rapidly strained flows and also has advantages over other turbulence models [24–27]. For the steady flow, the equations of the model k-ω SST are as follow:

$$\frac{\partial(\rho u_j k)}{\partial x_j} = P - \beta^* \rho \omega k + \frac{\partial}{\partial x_j}\left[(\mu + \sigma_k \mu_t)\frac{\partial k}{\partial x_j}\right] \quad (3)$$

where **x** is the spatial coordinates, k is the turbulence kinetic energy, P is the manifold pressure, β^* is the *SST* turbulence model constant, which is equal to 0.09, ω is the specific dissipation rate, μ is the molecular dynamic viscosity, σ_k is the k- ω turbulence model constant and u_T is the turbulent viscosity.

$$\frac{\partial(\rho\omega)}{\partial x_j} = \frac{\gamma}{v_t}P - \beta\rho\omega^2 + \frac{\partial}{\partial x_j}\left[(\mu + \sigma_\omega \mu_t)\frac{\partial \omega}{\partial x_j}\right] + 2(1-F_1)\frac{\rho\sigma_{\omega 2}}{\omega}\frac{\partial k}{\partial x_j}\frac{\partial \omega}{\partial x_j} \quad (4)$$

where:

$$P = \tau_{ij}\frac{\partial u_i}{\partial x_j} \quad (5)$$

$$\tau_{ij} = \mu_T\left(2S_{ij} - \frac{2}{3}\frac{\partial u_k}{\partial x_k}\delta_{ij}\right) - \frac{2}{3}\rho k\delta_{ij} \quad (6)$$

$$S_{ij} = \frac{1}{2}\left(\frac{\partial u_i}{\partial x_j} + \frac{\partial u_j}{\partial x_i}\right) \quad (7)$$

$$\mu_t = \frac{\rho a_1 k}{\max(a_1\omega, \Omega F_2)} \quad (8)$$

$$F_1 = \tanh(arg_1^4) \quad (9)$$

$$arg_1 = min\left[\max\left(\frac{\sqrt{k}}{\beta^*\omega d}, \frac{500v}{d^2\omega}\right), \frac{4\rho\sigma_{\omega 2}k}{CD_{k\omega}d^2}\right] \quad (10)$$

$$CD_{k\omega} = max\left(2\rho\sigma_{\omega^2}\frac{1}{\omega}\frac{\partial k}{\partial x_j}\frac{\partial \omega}{\partial x_j}, 10^{-20}\right) \quad (11)$$

$$F_2 = \tanh(arg_2^2) \quad (12)$$

$$arg_2 = \max\left(2\frac{\sqrt{k}}{\beta^*\omega d}, \frac{500v}{d^2\omega}\right) \quad (13)$$

$$\Omega = \sqrt{2W_{ij}W_{ij}} \quad (14)$$

$$W_{ij} = \frac{1}{2}\left(\frac{\partial u_i}{\partial x_j} - \frac{\partial u_j}{\partial x_i}\right) \quad (15)$$

where δ is the identity matrix or Kronecker Delta function, Ω is the vorticity magnitude.

The values of constants used for the two models are summarized in Table 3.

2.4.1. The far-field and limits conditions

For the far-field, the following conditions apply

$$\frac{U_\infty}{L} < \omega_{farfield} < 10\frac{U_\infty}{L}$$

$$\frac{10^{-5}U_\infty^2}{Re_L} < k_{farfield} < 10\frac{0.1U_\infty^2}{Re_L}$$

For the conditions at the limits /wall

$$\omega_{wall} = 10\frac{6v}{\beta_1(\Delta d_1)^2} \quad (16)$$

$$k_{wall} = 0$$

Table 3
The values of constants used in the two models of turbulence [26].

Designation	Constants/conditions	Values
k-ω model	σ_{k1}, $\sigma_{\omega 1}$, β_1	0.50, 0.650, 0.0750
k-ε model	σ_{k2}, $\sigma_{\omega 2}$, β_2	1.00, 0.856, 0.0828
SST model	β^*, a_1	0.09, 0.31

2.5. Boundary conditions

In this study, crude oil at 30° API is used with the physical properties determined at 150 °C and 1 atm, υ = 4.016 × 10^{-6} m^2/s and ρ = 783.218 kg/m^3 [24]. The velocity at the inlet of the head of the exchanger is 1.252 m/s, it is considered to be uniform and normal to the head input surface.

The flow condition for the output of the head is modeled using the Outflow condition.

The turbulence intensity ($0.16Re^{1/8}$) and the length scale ($0.07D_n$) are selected as input for the turbulence [27]. Here ***Re*** is Reynolds number and $\boldsymbol{D_n}$ is the nominal diameter.

2.7. Method of resolution

The performance of the heat exchanger has been evaluated by using the CFD package ANSYS Fluent 15.0. The simple algorithm has been chosen for the pressure-velocity coupling. As convergence criteria of each control volume, residues are imposed for a value which is less than 10^{-5}. The computation time required almost 36 h on a mobile workstation with an Intel processor I-7-3740 QM CPU and 2.70 GHz.

3. results and discussion

The studied heat exchanger is a typical industrial medium size, and it contains one pass with 464 tubes for the 90° arrangement [24]. For the other arrangements, the same parameters are used except the number of tubes and their pitches. The results of the CFD in this section are on the average time, due to the ergodicity of turbulent flow.

To validate the calculation procedure, the results obtained for the case of 90° arrangement are compared with those obtained analytically by Mohammadi and Malayeri [24]. The results (Fig. 4) are satisfying and are in agreement with the cited work.

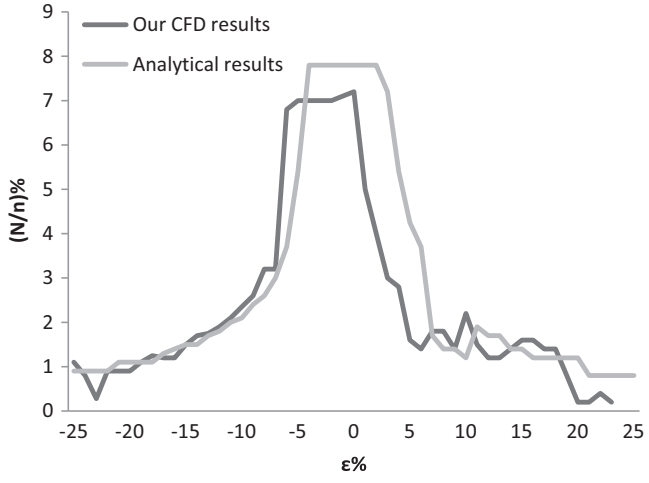

Fig. 4. CFD Validation.

Table 4
Remarkable velocities of all types of arrangements.

Type of arrangement	Highest velocity recorded in tube (m/s)	Lowest velocity recorded in tube (m/s)	Mean velocity (m/s)
90°	1.513	0.917	1.190
60°	1.627	0.697	1.167
45°	1.471	0.946	1.250
30°	1.118	0.905	1.096

Furthermore, the maximum velocity deviation | ε | is around 25%. The fluid velocity deviation ε is calculated by:

$$\varepsilon_i = \frac{U_i - U_m}{U_m} \tag{17}$$

where $\boldsymbol{U_i}$ the velocity at the tube i, and $\boldsymbol{U_m}$ is the mean velocity.

The important values of velocities for each type of arrangements are mentioned in Table 4. We note that, the 45° arrangement recorded the highest average velocity and the 30° arrangement has the lowest one. This is due to the configuration that has the lowest and highest number of tubes which can decrease or increase the tube resistance, which means that the heat exchangers with 45° arrangement types are the most economical because they have the lowest number of tubes and the most expensive are the heat exchangers with 30° arrangement types. In addition, the difference between lateral and transversal pitch directly influences the velocity distribution. Both highest and lowest velocity are recorded at the 60° arrangement (Fig. 6) with the values of 1.627 m/s and 0697 m/s, respectively.

Any variation of less than ± 5% in the average velocity can be ignored, and the corresponding flow distribution will be considered perfect [11,24]. The results obtained for the flow distribution are shown for different values of the ratio $\boldsymbol{N/n}$ as a function of velocity deviation. The flow distribution for different arrangement are shown in Figs. 5–8, where $\boldsymbol{N/n}$ is the ratio of the number of tubes having certain velocity deviation (Eq. (17)) referring to the total number of tubes. The uniformity of distribution curves can help in the design of shell and tube heat exchangers (STHeX), since they will give the information of the minimum total number of tubes for which an acceptable flow distribution can be achieved. Fig. 5 shows that the curve of flow distribution varies in the interval [−25%, 26%]: it is a little symmetric in the case of the arrangement of 90° but the dominant part is in the left side of the value of

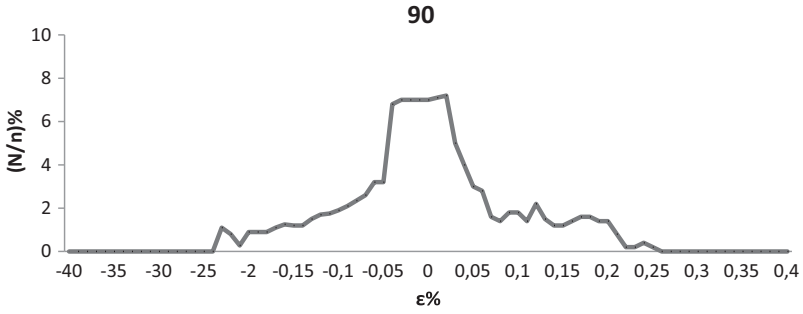

Fig. 5. Flow distribution curve for the 90° arrangement.

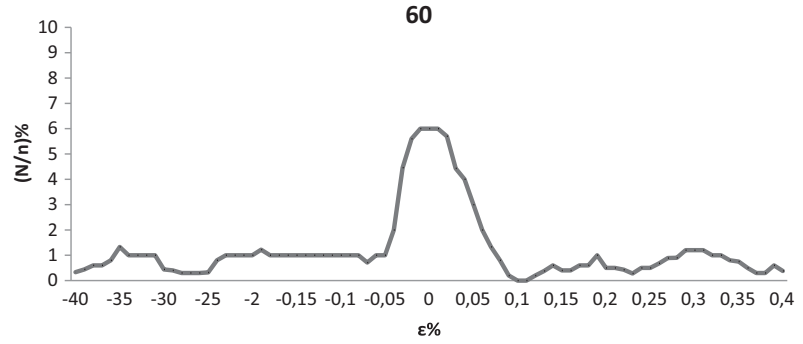

Fig. 6. Flow distribution curve for the 60° arrangement.

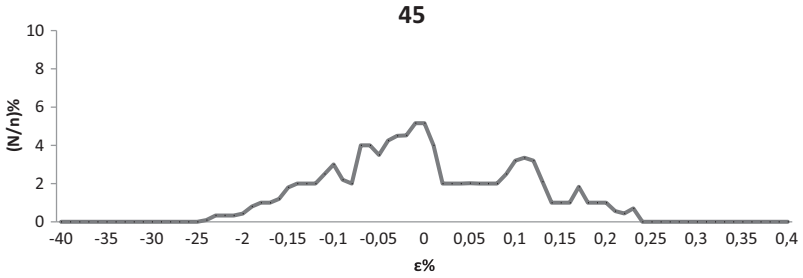

Fig. 7. Flow distribution curve for the 45° arrangement.

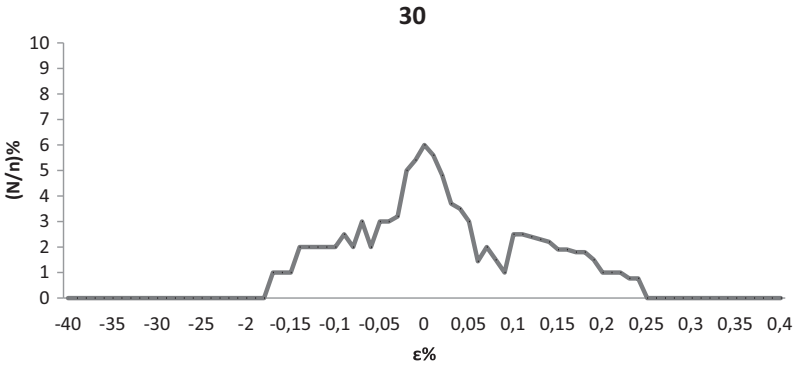

Fig. 8. Flow distribution curve for the 30° arrangement.

ε = 0. Fig. 6 (case of the arrangement of 60°) shows that the curve of flow distribution varies in the interval [−40%, 40%]: it is greater in the right side of the value of ε = 0, which means a large number of tube with a greater velocities of flow than the average velocity and that there is not a large number of tubes with a minimum flow velocity. By taking into account the value of the average velocity, the percentage of tubes with a minimum flow and the value the minimum velocity in the tubes, this arrangement may be recommended for fluids with low viscosity. It is clear that, in the case of the 45° arrangement (Fig. 7), the distribution of the flow varies between [−24%, 25%]: it is greater in the left side of the value of ε = 0, but the dominant part has a low velocity deviation (variation between [−15%, 0%]), which ensures a minimum flow. Fig. 8 (case of 30° arrangement) shows that the curve of flow distribution varies in the interval [−18%, 26%]: it is a little symmetric as the case of 90° arrangement. It is clear that the minimum value of the velocity deviation is not less than −18% nor superior than 26%, which means that there is not a large variation in the distribution of flows.

As previously mentioned, the maldistribution in the turbulent regime is not a function of the Reynolds number. However, the velocity deviation depends on the geometrical arrangement of the heat exchanger and may also depend on Reynolds number. The results show that the 60° arrangement is the most likely to give better uniformity of flow distribution, with over 46% of tubes with a velocity deviation $|\varepsilon| \leq 5\%$, indicating a high rate tube with a uniform distribution. This represent an enhancement of 21% compared to the conventional case of 90° arrangement. It is followed by the 30° arrangement which is almost the same case as the 90° arrangement and finally the 45° arrangement (Fig. 9).

It can be noted that for the 45° arrangement, over 33% of the tubes have a flow rate with a velocity deviation more than 5%. Those of the 30° arrangement come next with more than 29% of the tubes which have a velocity deviation greater than 5%, then those of the 90° arrangement with almost 26% with a deviation greater than 5% and in the last position, those of the 60° arrangement with more than 24% of tube (Fig. 10).

Another method of comparing between the conventional arrangement and the other arrangements (Fig. 11), which is proposed in this paper, can be defined by the addition of the percentage of tubes having velocity deviation varying between ±5% and the percentage of tubes having velocity deviation bigger than 5%.

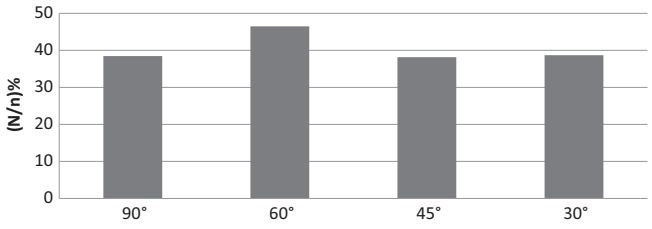

Fig. 9. Representation of flow distribution with $|\varepsilon| \leq 5\%$.

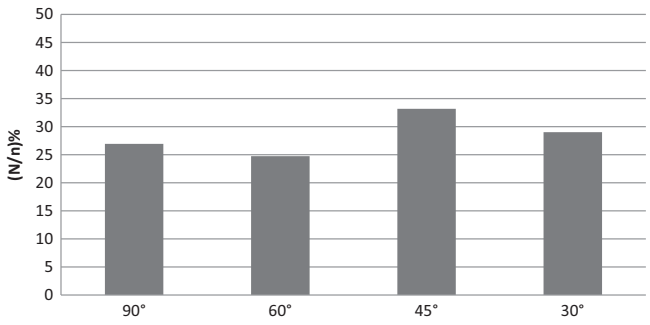

Fig. 10. Representation of flow distribution with $\varepsilon > 5\%$.

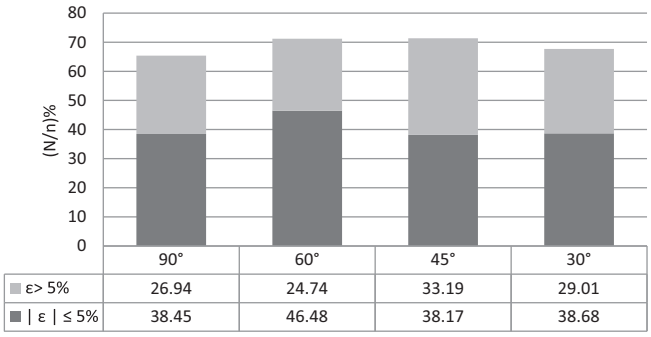

	90°	60°	45°	30°
ε> 5%	26.94	24.74	33.19	29.01
| ε | ≤ 5%	38.45	46.48	38.17	38.68

Fig. 11. Representation of flow distribution with $\varepsilon \geq -5\%$.

Table 5
Percentage of enhancement of fluid distribution.

Type of arrangement	Percentage of enhancement	Observation
45°	9.12%	-The most economical because of the lowest number of tubes.- High mean velocity- Recommended for fluid with high viscosity
60°	8.92%	- Large number of tubes with low flow velocity- recommended for fluid having low viscosity
30°	3.52%	- Higher number of tubes compared to the other type of arrangements

Table 5 presents the enhancement of fluid distribution of three arrangements (30°, 45° and 60°) compared to the conventional arrangement (90°). This results are obtained from Fig. 11.

4. Conclusion

A numerical simulation has been achieved to investigate the effect of the tubes arrangement on the flow distribution. The results show that the flow distribution is affected by the tubes arrangement type. The 45° arrangement ensures a high velocity at maximum number of tubes, which is recommended for high viscosity fluids as liquid. The 60° arrangement has a large number of tubes with low flow velocity, which is recommended for fluid having low viscosity (gas) due to their low ability of fouling. This arrangement gave the better flow distribution uniformity.

References

[1] B.I. Master, K.S. Chunangad, A. Boxma, D. Kral, P. Stehlik, Most frequently used heat exchangers from pioneering research to worldwide applications, Heat Transf. Eng. 27 (2006) 4–11.
[2] R. Brogan, Shell and tube heat exchangers, in, 2013.
[3] A. Mueller, Effects of some types of maldistribution on the performance of heat exchangers, Heat Transf. Eng. 8 (1987) 75–86.
[4] J.R. Thome, Eng. Data book III (2004).
[5] Q. Wang, Q. Chen, G. Chen, M. Zeng, Numerical investigation on combined multiple shell-pass shell-and-tube heat exchanger with continuous helical baffles, Internat. J. Heat Mass Transf. 52 (2009) 1214–1222.
[6] A. Acrivos, B. Babcock, R. Pigford, Flow distributions in manifolds, Chem. Eng. Sci. 10 (1959) 112–124.
[7] T. Kubo, T. Ueda, On the characteristics of divided flow and confluent flow in headers, Bullet. JSME 12 (1969) 802–809.
[8] G.R. Putnam, W.M. Rohsenow, Viscosity induced non-uniform flow in laminar flow heat exchangers, Internat. J. Heat Mass Transf. 28 (1985) 1031–1038.
[9] T. Kuppan, Heat exchanger design handbook, CRC, 2000.
[10] G. Mohan, B.P. Rao, S.K. Das, S. Pandiyan, N. Rajalakshmi, K. Dhathathreyan, analysis of flow maldistribution of fuel and oxidant in a PEMFC, J. Energy Resource. Tech. 126 (2004) 262–270.
[11] G.F. Hewitt, J. Barbosa, Heat exchanger design handbook, Begell House, 2008.
[12] L. Fang, Y.-H. LUO, S.-M. YANG, Analytical and experimental investigation of flow distribution in manifolds for heat exchangers*, J. Hydrodynam., Ser. B 20 (2008) 179–185.
[13] M. Saber, J.-M. Commenge, L. Falk, Rapid design of channel multi-scale networks with minimum flow maldistribution, Chem. Eng. Process. Process Intensificat. 48 (2009) 723–733.
[14] L.-Z. Zhang, Flow maldistribution and thermal performance deterioration in a cross-flow air to air heat exchanger with plate-fin cores, Internat. J. Heat Mass Transf. 52 (2009) 4500–4509.
[15] L.-Z. Zhang, Performance deteriorations from flow maldistribution in air-to-air heat exchangers: a parallel-plates membrane core case, Numeric. Heat Transfer, Part A: Appl. 56 (2009) 746–763.
[16] J. Wang, Pressure drop and flow distribution in parallel-channel configurations of fuel cells: Z-type arrangement, Internat. J. Hydrogen Energy 35 (2010) 5498–5509.
[17] J. Wang, Theory of flow distribution in manifolds, Chem. Eng. J. 168 (2011) 1331–1345.
[18] E.V. Rebrov, J.C. Schouten, M.H. De Croon, Single-phase fluid flow distribution and heat transfer in microstructured reactors, Chem. Eng. Sci. 66 (2011) 1374–1393.
[19] Y. Venkatesan, Effect of maldistribution and flow rotation on the shell side heat transfer in a shell and tube heat exchanger, in, Wichita State University, 2011.
[20] M.M.A. Bhutta, N. Hayat, M.H. Bashir, A.R. Khan, K.N. Ahmad, S. Khan, CFD applications in various heat exchangers design: a review, Appl. Therm. Eng. 32 (2012) 1–12.
[21] M.S. Gandhi, A.A. Ganguli, J.B. Joshi, P.K. Vijayan, CFD simulation for steam distribution in header and tube assemblies, Chem. Eng. Res. Design 90 (2012) 487–506.
[22] L.-Z. Zhang, Z.-X. Li, T.-S. Zhong, L.-X. Pei, Flow maldistribution and performance deteriorations in a cross flow hollow fiber membrane module for air humidification, J. Memb. Sci. 427 (2013) 1–9.
[23] Z.-X. Li, L.-Z. Zhang, Flow maldistribution and performance deteriorations in a counter flow hollow fiber membrane module for air humidification/dehumidification, Internat. J. Heat Mass Transf. 74 (2014) 421–430.
[24] K. Mohammadi, M. Malayeri, Parametric study of gross flow maldistribution in a single-pass shell and tube heat exchanger in turbulent regime, Internat. J. Heat Fluid Flow 44 (2013) 14–27.
[25] D.C. Wilcox, Turbulence modeling for CFD, DCW industries La Canada, CA, 1998.
[26] F.R. Menter, Two-equation eddy-viscosity turbulence models for engineering applications, AIAA journal 32 (1994) 1598–1605.
[27] F.U.s. Guide, Version 15, ANSYS, Inc., April, (2014).